Appl. Phys. B 62, 407–413 (1996)

Applied Physics B Lasers and Optics

Gas-phase velocimetry by nearly degenerate four-wave mixing

P. M. Danehy[1], R. L. Farrow[2]

[1] High Temperature Gasdynamics Laboratory, Stanford University, Stanford, CA 94305-3032, USA
(Fax 415/723-1748)
[2] Combustion Research Facility, Sandia National Laboratories, Livermore, CA 94551-0969, USA

Received: 29 May 1995/Accepted: 12 September 1995

Abstract. We demonstrate a new velocimetry technique for gas flows based on Nearly Degenerate Four-Wave Mixing (NDFWM). Measurements were performed on nitric oxide in a free-jet expansion using helium and argon as carrier gases, at flow velocities on the order of 1000 m/s. We obtained velocities by analyzing experimental spectra from the jet using a perturbative treatment of NDFWM that we extended to include an arbitrary bulk velocity. The results agreed with independent velocity measurements based on Laser-Induced Fluorescence (LIF), as well as with theoretical flow-field velocities, to better than 5% in all cases studied.

PACS: 06.30Gv; 42.65. – k; 42.62.Fi

Flow velocity is a critical parameter in many scientific and technological applications. Velocimetry has developed from the early use of intrusive physical probes such as pitot tubes and hot-wire anemometers [1] to non-intrusive optical techniques such as Laser-Doppler Velocimetry (LDV) [1] and Particle Image Velocimetry (PIV) [2]. LDV is capable of precise measurements from a small probe volume ($< 10^{-3}$ cm^{-3}) while PIV provides two-dimensional velocity maps. However, both methods require seeding of the flow with particles, leading to the possibilities of particles perturbing the flow or failing to follow the flow with sufficient accuracy. Optical techniques based on molecular tracers (either present in the flow or added in low concentrations) are often preferable to LDV and PIV for these reasons. Some of these techniques "tag" molecules with a laser and map the convected distribution after a fixed time delay [3, 4]. Using a different approach, spectroscopic velocimetry techniques exploit the Doppler shifts of atomic or molecular spectral features. For example, spectral shifts in absorption have been used for path-integrated velocimetry [4]. Laser-Induced Fluorescence (LIF) has been used to perform velocimetry simultaneously with temperature and pressure measurements in a small volume [5]. Flow fields have been mapped using Doppler shifts in planar LIF [6] and Rayleigh scattering [7].

Velocimetry based on coherent, nonlinear optical processes has recently been reported [8, 9]. Such techniques offer several advantages compared to conventional (non-coherent) methods. The collimated, spectrally bright signal beams obtained with coherent techniques are useful in harsh environments: spectral and spatial filtering of the signals to attenuate luminosity and spurious scattered light can be performed with minimal losses. The ability to remotely detect the collimated signal beam is advantageous when heat, electrical interference, or other hostile conditions are present at the sample region [10]. Lefebvre et al. [8] have demonstrated four-wave mixing velocimetry based on Coherent Anti-Stokes Raman Spectroscopy (CARS). This method provides instantaneous gas velocity and temperature within a focused beam volume ≈ 30 mm in length, oriented approximately parallel to the flow. Williams et al. [9] recently demonstrated gas-phase velocimetry using Degenerate Four-Wave Mixing (DFWM). Using a forward-beam phase-matching geometry, Williams et al. similarly obtained an extended probe volume (≈ 20 mm) oriented along the flow direction. In principle this method can provide velocities from single laser pulses, using broadband DFWM techniques [11].

In this paper we report a velocimetry method based on Nearly Degenerate Four-Wave-Mixing (NDFWM). The method contrasts with the previously described FWM techniques in that the crossed laser beams are directed mostly perpendicular to the flow. This geometry may be advantageous in applications where optical accessibility along the flow direction is limited. A relatively large beam-crossing angle is employed to gain velocity sensitivity, resulting in improved spatial resolution (≈ 2 mm interaction length). The NDFWM technique will be shown to have potentially greater spectral sensitivity to velocity than LIF. The velocity sensitivity, as defined by a spectral shift-to-width ratio, is greater for NDFWM as it has a sub-Doppler spectral linewidth at small beam angles. In addition, NDFWM is applicable to non-fluorescing species since it relies on absorption rather than emission.

We have experimentally demonstrated the NDFWM technique in a simple, well-understood flow: a free jet expanding into a vacuum. We have also performed velocity measurements using LIF at the same conditions as NDFWM and have compared the results to theoretical predictions of the flow field.

1 Approach

Two laser beams of nearly the same frequency are crossed in a flowing absorbing medium, resulting in a sinusoidal interference pattern in the total optical field. The fringes are not stationary but move with a velocity proportional to the relative spectral detuning. If the medium has a nonlinear susceptibility, the fringes induce a sinusoidal perturbation in the index of refraction and absorption coefficient of the flowing gas. The amplitude of the perturbation is enhanced when the flow velocity, projected onto the propagation direction of the fringes, matches the fringe velocity. (In this case the flow does not wash out the fringes.) A third incident laser beam partially diffracts from the grating to produce the signal beam. The flow velocity is determined from the frequency detuning that produces the maximum diffracted signal. This effect is observed in the NDFWM detuning spectrum as a shift in peak position proportional to velocity. An expression involving the beam-crossing angle and laser frequency relates the shift to the velocity. It is possible to direct additional beams into the sample region to obtain new beam interference patterns and thus different fringe velocities and propagation directions. With the correct phase-matching, these additional gratings can be used to measure different projections of the flow velocity.

The analysis of NDFWM spectra of a flowing gas is based on the perturbative treatment of NDFWM by Nilsen and Yariv [12]. We extended the treatment to include arbitrary bulk velocities, $\mathbf{V}_{\text{bulk}} = \{V_{\text{bulk},x}, V_{\text{bulk},y}, V_{\text{bulk},z}\}$. Figure 1a shows the beam geometry used in the calculation (and experiment) relative to the free-jet expansion. The forward- and backward-pump frequencies are fixed to the center of the (stationary molecule) absorption line [12]. We computed NDFWM signal intensities for this case as a function of probe detuning using

$$I_{\text{NDFWM}}(v) \propto \left| \int_{-\infty}^{\infty} \rho(\mathbf{v}_N)\kappa(\mathbf{v}_N, v)\, \mathrm{d}^3 v_N \right|^2, \tag{1}$$

where the Maxwellian velocity distribution, $\rho(\mathbf{v}_N)$, is

$$\rho(\mathbf{v}_N) = \frac{1}{(\pi u_N^2)^{3/2}} \exp\left[-(|\mathbf{v}_N - \mathbf{V}_b|^2/u_N^2)\right] \tag{2}$$

and the velocity-dependent nonlinear coupling coefficient, $\kappa(\mathbf{v}_N, v)$, is given by

$$\begin{aligned}\kappa(\mathbf{v}_N, v) = \frac{-\alpha_0}{2}\frac{A_f A_b}{E_s^2}\Bigg(&\frac{i}{(\hat{n}_f\cdot\mathbf{v}_N + i)[1 - iav + ia\mathbf{v}_N\cdot(\hat{n}_p - \hat{n}_f)](v + \hat{n}_s\cdot\mathbf{v}_N + i)} \\ &+ \frac{i}{(\hat{n}_b\cdot\mathbf{v}_N + i)[1 - iav + ia\mathbf{v}_N\cdot(\hat{n}_p - \hat{n}_b)](v + \hat{n}_s\cdot\mathbf{v}_N + i)} \\ &+ \frac{i}{(v - \hat{n}_p\cdot\mathbf{v}_N + i)[1 - iav + ia\mathbf{v}_N\cdot(\hat{n}_p - \hat{n}_f)](v + \hat{n}_s\cdot\mathbf{v}_N + i)} \\ &+ \frac{i}{(v - \hat{n}_p\cdot\mathbf{v}_N + i)[1 - iav + ia\mathbf{v}_N\cdot(\hat{n}_p - \hat{n}_b)](v + \hat{n}_s\cdot\mathbf{v}_N + i)}\Bigg)\end{aligned} \tag{3}$$

where

ω_0 = center frequency of resonance (stationary molecules)
ω_i = frequency of beam i
γ_{12} = homogeneous linewidth (hwhm)
$v = (\omega_p - \omega_0)/\gamma_{12}$ = normalized detuning of probe from line center
$\mathbf{v}_N = \omega_0\mathbf{v}/(c\gamma_{12})$ = normalized velocity
$\mathbf{V}_{N\text{bulk}} = \omega_0\mathbf{V}_{\text{bulk}}/(c\gamma_{12})$ = normalized bulk flow velocity
$u_N = \omega_0 u_{mp}/(c\gamma_{12})$ = normalized most probable thermal velocity
$\hat{n}_i = \mathbf{k}_i/(2\pi\omega_0)$ = normalized wave vector for beam i
$a = \gamma_{12}/\Gamma_0$ (where Γ_0 is the population decay rate)
α_0 = line-center absorption coefficient
E_s = line-center saturation field
A_i = field amplitude of beam i
c = speed of light.

The subscripts f, b, p, and s on the terms A_i, ω_i, and $\hat{n}_i$ correspond to the forward-pump, backward-pump, probe, and signal beams, respectively. The parameter u_N is exactly the inverse of the "a" parameter used in the Voigt spectral profile [13]. Note that this treatment is valid for low incident laser intensities only; to our knowledge, a non-perturbative theory of NDFWM that simultaneously includes collisional and Doppler broadening and saturation is not presently available.

By combining and directly integrating (1) –(3) as a function of detuning for the geometry of Fig. 1, we obtained theoretical NDFWM spectra for arbitrary values of $\mathbf{V}_{\text{bulk}}$. We investigated the variation of the resonance peak position with the magnitude and direction of $\mathbf{V}_{\text{bulk}}$ as well as with the beam-crossing angle, Θ, and found that the spectral shift of the resonance was given to within one percent by

$$\Delta\omega_{\text{shift}} = \frac{\omega_0 V_{\text{bulk},z}\sin\Theta}{c}, \tag{4}$$

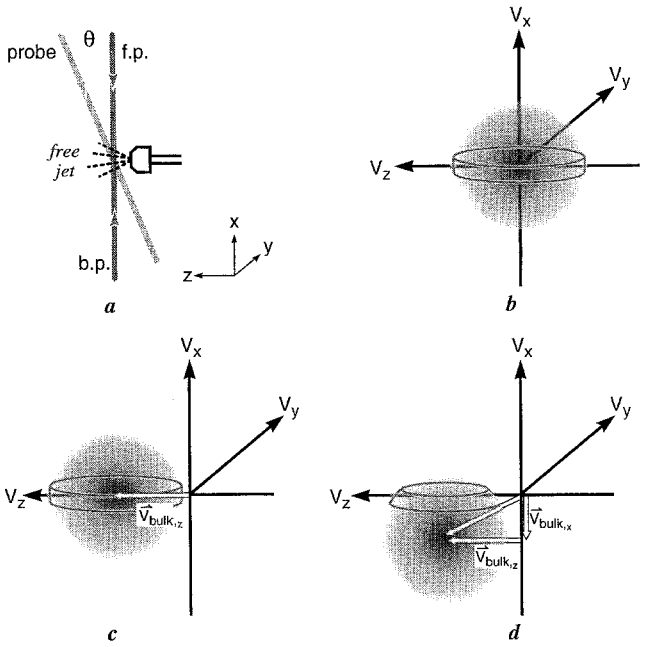

Fig. 1a–d. Beam geometry and velocity-group selection by the pump beams. **a** The forward-pump (f.p.), backward-pump (b.p.) and probe beams intersect in the jet, **b** Shows the Maxwellian distribution in velocity space for the case of $V_{\text{bulk},z} = V_{\text{bulk},x} = 0$. **c** Shows shifted distribution for the case of $V_{\text{bulk},z} \neq 0$, $V_{\text{bulk},x} = 0$. **d** Shows the case of $V_{\text{bulk},z} \neq 0$, $V_{\text{bulk},x} \neq 0$. In each case, the disk-shaped region highlights the pump-selected velocity group, and $V_{\text{bulk},y} = 0$

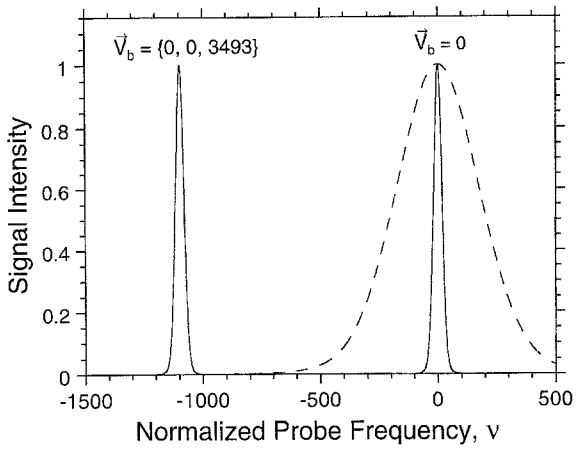

Fig. 2. Theoretical NDFWM spectra with $\mathbf{V}_{\text{Nbulk}} = 0$ (*solid line, right*) and $\mathbf{V}_{\text{Nbulk}} = \{0, 0, 3493\}$ (*solid line, left*). The *dashed line* corresponds to $\mathbf{V}_{\text{Nbulk}} = 0$ with the frequency scale expanded by a factor of 10 to clarify the line shape. The probe detuning is given in the normalized frequency units described in the text

for the following range of conditions

$$\frac{u_N^{0.8}\sqrt{V_{\text{Nbulk},x}^2 + V_{\text{Nbulk},z}^2}}{|V_{\text{Nbulk},x}|} > 60 \tag{5}$$

Thus, if the direction of the flow is orthogonal to the pump beams ($V_{\text{Nbulk},x} = 0$), then (4) gives the observed shift, regardless of the dominant broadening mechanism. On the other hand, if the system is Doppler broadened ($u_N \gg 1$), then (4) applies for $V_{\text{Nbulk},x} \neq 0$ as long as (5) is obeyed.

Figure 2 shows a sample calculation for two values of $\mathbf{V}_{\text{bulk}}$ with helium as the carrier gas. We estimated the properties in the effusive jet by calculating temperature, velocity, and number density according to well-known gasdynamic relations [14]. The calculation corresponds to conditions on the jet axis, at $x/D = 15$ (where D is the diameter of the nozzle) where $T = 2.27$ K, $P = 11.9$ Torr, $\mathbf{V}_{\text{bulk}} = \{0, 0, 1744 \text{ m/s}\}$, $u_{mp} = 35.3$ m/s, $\Delta\nu_{\text{Doppler}} = 0.0087 \text{ cm}^{-1}$, and $2\gamma_{12} = 0.00015 \text{ cm}^{-1}$ (the latter is dominated by radiative decay from the NO A state and from time-of-flight broadening). These conditions correspond to $\mathbf{V}_{\text{Nbulk}} = \{0, 0, 3493\}$, $u_N = 71$, and $a = 1$ in the dimensionless parameters introduced above. A small measurement volume was assumed.

The narrow peak centered on zero in Fig. 2 shows the spectrum calculated by scanning the probe frequency with $\mathbf{V}_{\text{Nbulk}} = \{0, 0, 0\}$. The narrow peak on the left corresponds to the calculation for $\mathbf{V}_{\text{Nbulk}} = \{0, 0, 3493\}$. Note that the spacing between the peaks agrees with (4). Furthermore, the linewidth is dominated by residual Doppler broadening: the width (hwhm) is ~20 normalized units. (Since the units are normalized by γ_{12}, the observed width is ~20 times greater than the homogeneous broadening.) The dashed peak centered on zero is the same calculation expanded by a factor of ten to reveal the Gaussian shape of the spectral feature.

Considering the interaction of the three laser beams with particular velocity groups in the flow helps to form a physical interpretation of these results. As mentioned above, the forward- and backward-pump beams (derived from the same laser) are tuned to the center of an absorption transition for non-Doppler shifted molecules. In a Doppler-broadened medium, the pump beams will be resonant only with molecules having near-zero velocity in the x-direction (the disk-shaped region in velocity space shown in Fig. 1b). We neglect interactions with other velocity classes since they can resonate with one beam at most (the probe). Because the probe crosses the pump beams at a non-zero angle Θ, molecules resonant with the pumps can have a non-zero velocity projection on the probe beam. The probe can resonate with these molecules when its frequency is detuned by the appropriate Doppler shift. Thus, the resonance peak obtained by tuning the probe is Doppler shifted according to the velocity of the selected molecules as projected on the probe team.

For example, if the gas has zero bulk velocity (Fig. 1b), then the selected Maxwellian (for instance) distribution is centered on zero and the peak signal will be observed at zero detuning (consistent with (4)). On the other hand, if the gas has a component of bulk velocity in the z-direction, then the Maxwellian distribution is centered at $v_z = \mathbf{V}_{\text{bulk},z}$ (Fig. 1c) and the signal intensity will have a peak at a frequency given by (4). This spectral shift corresponds to the Doppler shift of pump-selected molecules with velocity projected on the probe beam. In the case of a component of the bulk velocity in the x-direction (Fig. 1d), the pump beams again select the molecules (now in the wings of the distribution) which have near-zero

x-velocity. Again, the signal has a peak resonance according to (4). The pump beams isolate the z-component of the velocity vector, and the probe determines the magnitude of this vector by observing the Doppler shift as the probe frequency is tuned. Thus, the technique measures the component of the gas velocity orthogonal to the pump beams. This optical configuration allows velocity measurements without optical access along the flow direction.

A description of the technique based on the concept of laser-induced gratings provides additional insight. The forward-pump and probe beams cross, generating interference fringes in the free-jet expansion. Since these two beams have different frequencies, the fringes move in the z-direction with a velocity given by the following equation:

$$V_{\text{fringes},z} = \frac{(\omega_2 - \omega_1)c}{\omega_0 \sin\Theta} \tag{6}$$

where ω_1 and ω_2 are the frequencies of the two laser beams and Θ is the angle between the forward-pump and probe beams. This expression is equivalent to (4) with the substitutions: $V_{\text{bulk},z} = V_{\text{fringes},z}$, $\Delta\omega_{\text{shift}} = \omega_2 - \omega_1$ and with ω_0 equal to the average frequency of the two lasers instead of the molecular resonance frequency. When the velocity of the fringes matches the velocity of the absorbing medium, a moving grating will be most efficiently written into the flow. (In the molecular frame of reference the grating is stationary, leading to the longest lifetime and consequently the greatest amplitude.) As this absorption perturbation convects with the flow, it diffracts a small portion of the backward-pump beam in the direction of the probe beam, generating a collimated, coherent signal beam. Again, the frequency shift, and hence the velocity, is found by measuring the signal intensity while scanning the frequency of the probe beam.

Performing the experiment as described above results in a single-peaked spectrum. Accurate measurements of the probe frequency relative to that of the pumps are necessary to obtain the resonance shift needed to compute the velocity. Such measurements can be performed using a precise wavemeter or by calibrating against low-pressure LIF spectra of molecules in a static cell. However, with only slightly more experimental effort, we made the NDFWM velocimetry technique described above self-calibrating. We precisely retro-reflected both the probe and forward-pump beams so that they passed through the flow a second time in a counter-propagating direction. This generated a new grating which moved at the same speed as, but in the opposite direction from, the original grating. In this geometry, the backward-pump beam is properly phase-matched to diffract from the new grating, generating an NDFWM signal beam collinear with the original one and allowing the use of a single detector for both beams. By tuning the probe, we obtained a two-peaked spectrum, in which the observed peak separation was exactly twice that predicted by (4).

In principle, when the NDFWM line shape is dominated by (residual) Doppler broadening, the technique can be used to measure the velocity and kinetic temperature of the gas simultaneously. Doppler broadening dominates the NDFWM line shape when all three of the following conditions are satisfied: the medium is Doppler-broadened, the beam-crossing angle Θ is large, and saturation broadening is small. In the present experiment, temperature could not be measured since saturation broadening and the laser linewidth masked the residual Doppler broadening (calculated to be $\approx 0.003\,\text{cm}^{-1}$ for the conditions of Fig. 2).

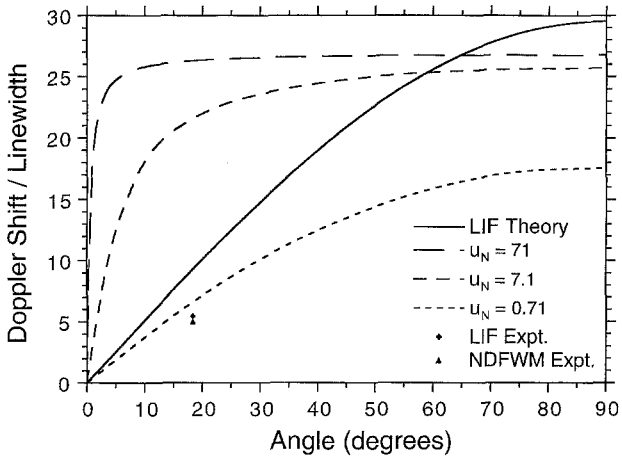

Fig. 3. Ratio of Doppler shift to observed spectral width vs forward-pump/probe beam angle. The *solid line* is the calculated ratio of LIF velocimetry, where zero degrees corresponds to the laser beam oriented orthogonally to the flow direction. The *long*, *intermediate*, and *short dashes* are for the NDFWM technique, calculated for $u_N = 71$, 7.1, and 0.71 respectively. Experimental LIF (*diamond*) and NDFWM (*triangle*) ratios are also shown

As an indication of the potential precision of spectroscopic velocimetry, we consider the ratio of Doppler shift to the observed linewidth; a large ratio facilitates measurements of the line shift. (The quality of the experimental spectra is also an important factor.) In Fig. 3, we have plotted the shift-to-width ratio for both LIF and NDFWM as a function of observation angle for the conditions of this experiment, again using helium as the carrier gas. Calculation of the shift-to-width ratio for LIF is based on a Voigt profile for the absorption line. The spectral width of the feature is constant with respect to observation angle. The Doppler shift simply increases as $\sin(\Theta)$ from $\Theta = 0°$ (flow perpendicular to laser beam) to 90° (flow parallel to beam). For the same conditions, labeled in Fig. 3 an $u_N = 71$, we have calculated the shift-to-width ratio for the NDFWM velocimetry technique using (1)–(3). For large observation angles, the shift-to-width ratio is comparable to that of LIF. However, NDFWM exhibits a much larger sensitivity at small angles. While the shift in the NDFWM spectra scales as $\sin(\Theta)$ according to (4), so does the spectral width at large angles. Thus, shift-to-width ratio is roughly constant expect at very small angles, where the linewidth is determined by homogeneous broadening. The persistence of the large shift-to-width ratio at small angles is particularly advantageous where optical access is limited. But, the corresponding small shifts can require very accurate frequency measurement and high-resolution lasers. The sub-Doppler linewidth at small beam-crossing angles is often exploited for high-resolution spectroscopy using DFWM [15].

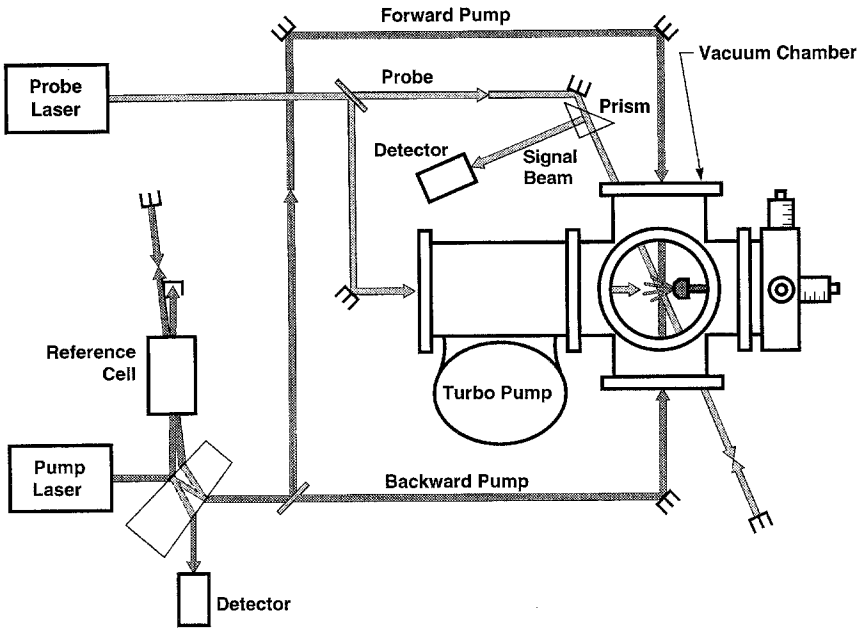

Fig. 4. Schematic diagram of the experiment. DFWM is performed in the reference cell by using an uncoated, wedged, quartz beam splitter (not drawn to scale) to generate the DFWM forward-pump and probe beams. NDFWM velocimetry is performed in the vacuum chamber. In the figure, "probe laser" and "pump laser" refer to the pulse-dye amplified laser systems described in the text

The curves in Fig. 3 labeled with larger values of u_N represent calculations performed for the same bulk velocity and temperature as for $u_N = 71$, but with different values of homogeneous broadening. Values of $u_N = 7.1$ and $u_N = 0.71$ correspond to homogeneous broadening 10 and 100 times higher than that of the experiment. Clearly, the velocity precision will be reduced in these cases. Recall that the theoretical development outlined above does not include the effects of saturation of the molecular transition. But, qualitatively, saturation is similar to pressure broadening in that both processes result in homogeneous broadening. Thus, smaller values of u_N indicate the trends expected from saturation: a reduction of the shift-to-width ratio and a corresponding decrease in the sensitivity to velocity.

2 Experiment

Figure 4 is a schematic diagram of the experiment. A turbo-molecular pump evacuated an eight-inch, six-way Conflat cross to a pressure of less than 1 m Torr. We used a piezo-electric pulsed nozzle with a diameter of 1 mm (Lasertechnics, model LPV) to generate pulses of 1% NO in carrier gases of He and Ar at 20 Hz. The nozzle was suspended horizontally from an x, y, z translation stage (shown in Fig. 4) with vacuum feed-throughs to allow accurate positioning of the jet. To generate an effusive jet with little velocity structure, we used a high backing pressure of 2200 torr. The gas velocity reached 98% of terminal velocity ($V_{term} = \sqrt{2c_pT}$) by $x/D = 5$. We performed measurements on the centerline-axis at $x/D = 15$ in the jet. For these conditions, gas velocities were calculated from gasdynamic theory [14] and they appear in Table 1.

We obtained the laser radiation used for the measurements by frequency doubling and mixing the outputs of two pulse-amplified ring lasers. For the probe laser, a cw single-mode ring-dye laser (Coherent 699-29) operating near 575 nm was amplified using three visible-dye cells pumped by a frequency-doubled Nd:YAG laser. We frequency-doubled the amplified light and mixed it with residual Nd:YAG laser fundamental to obtain single-mode pulses near 226 nm. For the lump laser, we used a cw single-mode Ti:Sapphire ring laser (Coherent 899-29) pulse-amplified using three near-IR-dye cells. The output was frequency-doubled and mixed with residual Nd:YAG second-harmonic to obtain radiation near 226 nm for the pump beams. The maximum pulse energies from the two systems were 1.25 and 0.25 mJ, respectively; both had pulse durations of 8–10 ns and FWHM bandwidths of $\sim 0.0035\ cm^{-1}$. For each spectral data point, the probe laser frequency was stepped $0.0007\ cm^{-1}$ and the results of 20–60 pulses were measured and averaged. We calibrated the frequency scan using a visible confocal etalon with a free-spectral range of $0.025\ cm^{-1}$.

We apertured the beams to 0.3 mm × 2.0 mm immediately adjacent to the test chamber. They crossed at an angle of 18.3° in the cell, resulting in a probe volume of 1.9 mm × 2.0 mm × 0.3 mm for the x, y, and z dimensions, respectively. Thus, the spatial resolution in the flow direction was 0.3 mm. All beams had vertical polarizations. We used ~1 μJ in the pump beams and ~0.1 μJ in the probe beam. The forward-pump and probe beams propagated in a horizontal plane. The backward-pump beam was angled

Table 1. Summary of results.

Gas	Theory	LIF	% diff.	NDFWM	% diff.
Argon	551.9	557	+ 0.9	534	− 3.1
Helium	1744.2	1663	− 4.7	1723	− 1.2

Note: All velocities are given in m/s. The percentage difference between theoretical and measured velocities is given by "% diff."

downward slightly, causing the signal beam to propagate at a slight downward angle with respect to the incident probe. We aligned the beams by placing a thin (2 mm) dye cell containing Coumarin 450 dye in ethanol in the beam intersection region, directly in front of the nozzle. When the lasers were tuned to precisely the same frequency, a DFWM signal was visible on a fluorescent card. We folded the signal beam with a prism and directed it through a 25 μm spatial filter onto a photomulitplier tube. As described above, we retro-reflected the forward-pump and probe beams in the horizontal plane to generate the second moving grating. An interference filter was placed in front of the NDFWM detector ($\lambda_{\text{center}} = 220$ nm, $\Delta\lambda_{\text{bandpass}} = 23$ nm). We performed measurements on the well-isolated $R_1(0)$ line of the $A^2\Sigma^+(v' = 0) \leftarrow X^2\Pi(v'' = 0)$ band of NO. This relatively weak transition was chosen to reduce saturation ($E_s^2 \propto 1/\sigma$, where σ is the transition absorption cross section) and to ensure interaction with a well-populated state.

As an independent measurement of the velocity of the jet, LIF was collected through a window above the sample region using a 0.3 mm slit aperture aligned with the axis of the jet. We generated self-calibrated LIF spectra by observing LIF from both the incident probe beam and the retro-reflected probe beam. By placing an interference filter in front of the LIF detector ($\lambda_{\text{center}} = 250$ nm, $\Delta\lambda_{\text{bandpass}} = 10$ nm) we selected emission from rotational transitions in the $A^2\Sigma^+(v' = 0) \rightarrow X^2\Pi(v'' = 2)$ band near 247 nm. The LIF and NDFWM measurements were not performed simultaneously.

To ensure that the NDFWM pump frequency was accurately tuned to the absorption line center for stationary molecules, we split off a fraction of the pump beam to perform DFWM in a small reference cell (Fig. 4). The cell had opposing fused-silica windows spaced 13 cm apart and was filled with 30 m Torr of NO and 3 Torr of He. The forward-pump and probe beams for DFWM were obtained from front- and back-square reflections from the single, wedged beam splitter. The latter also served to separate the phase-conjugate signal from the probe beam. By observing the signal in real time on an oscilloscope we were able to repeatably tune the pump frequency to within $\sim 0.005\ \text{cm}^{-1}$ of the NO line center. This method of molecular-frequency referencing is attractive compared to other sub-Doppler techniques such as Lamb-dip fluorescence, intermodulated fluorescence and saturated absorption since it provides an easily observed null-background signal. In addition, DFWM is applicable to non-fluorescing molecules.

3 Results

Sample experimental spectra, along with fits, appear in Fig. 5. The measurement location was on the jet centerline at $x/D = 15$, where essentially a single velocity class was probed satisfying (5). As expected, each spectral scan shows two distinct peaks. The splitting of the peaks is expected to be twice the Doppler shift, or twice $\Delta\omega_{\text{shift}}$ calculated from (4). We extracted the best-fit peak separation by fitting Voigt profiles to the features. (The experimental line shapes were dominated by saturation so that

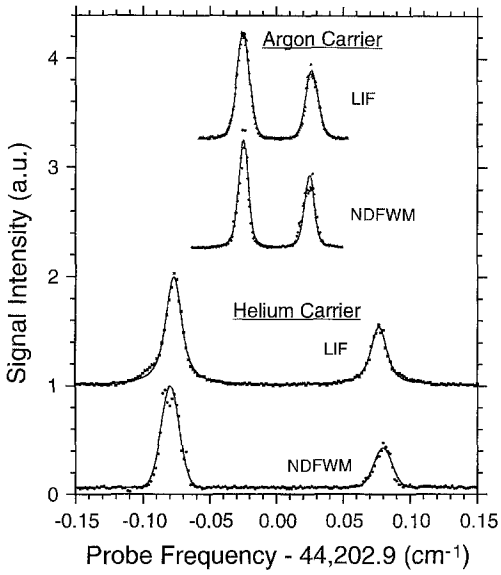

Fig. 5. Experimental NDFWM and LIF spectra of the $R_1(0)$ transition of NO measured in a pulsed jet. The data are indicated by symbols. Best-fit Voigt profiles are shown as *solid lines*. The splitting between the peaks is a measure of the flow velocity

fitting the spectra using (1)–(3) above was not feasible.) As Table 1 shows, the results of both LIF and DFWM agree with the theoretical velocities to better than 5% in all cases studied.

The precision of the measurements was limited both by experimental constraints and intentional trade-offs. To minimize saturation broadening in the NDFWM spectra, we used the lowest practical laser intensities. We used small beam diameters to improve the spatial resolution, resulting in a small sample volume. Furthermore, a large angle was used between the forward-pump and probe beams to maximize the observed Doppler shift, again reducing the sample volume. Thus, we traded off signal strength to gain velocimetric and spatial precision. Despite these precautions the observed spectral linewidths were larger than expected, limiting both precision and accuracy. In the case of NDFWM the observed widths were 5.3 times larger than predicted for the case of helium and 2.6 times larger for the case of argon. The LIF widths were also broader than expected: 1.7 times larger for helium and 1.3 times larger for argon. As a result, the experimental shift-to-width ratios achieved with both techniques were comparable, and were smaller than the predicted values (see data points in Fig. 3). The extra width resulted mainly from the laser linewidth and saturation broadening. The laser linewidth ($\sim 0.0035\ \text{cm}^{-1}$) accounted for approximately 40% of the broadening in the case of the narrowest observed linewidth (NDFWM in argon carrier). Thus, saturation was a significant limitation in this experiment, not surprising, considering the near-absence of collisional relaxation. (In applications involving higher pressures, saturation may be less important.) The discrepancy between theoretical and experimental values for LIF could have also resulted from misalignment of the viewing aperture relative to the centerline of the jet. This could have caused the LIF

detector to observe emission from an off-axis velocity group corresponding to a different Doppler shift.

For a fixed beam-crossing angle and/or flow direction, the minimum detectable velocity v_{min} is proportional to the observed linewidth for both LIF and NDFWM. Estimating our minimum detectable line shift to be 0.2 linewidths, we calculate $v_{min} \approx 90$ m/s in our NDFWM setup with He carrier gas. From (1) –(3) the linewidth for NDFWM with a non-zero crossing angle should vary as a Voigt profile: $\propto P^0 T^{1/2}$ in the Doppler-broadened limit and approximately $\propto PT^{-1/2}$ in the pressure-broadened limit. Thus, at room temperature but at low pressures, v_{min} would be 11.5 times larger, or 1000 m/s. Obviously, higher pressure flows would also be impractical. It is evident that flows at low densities and/or low temperatures are most suitable for velocimetry using NDFWM.

The current experimental setup is obviously too complex and expensive for practical applications, mainly due to the laser sources required. However, the development of inexpensive, compact, solid-state laser sources with output in the uv could alleviate this problem in the future. Such sources are currently applicable for tracer species absorbing in the visible and near-ir, e.g., certain rare-earth or halogenic atoms and molecules. In principle, the current technique could be extended to single-laser-pulse velocity measurements by substituting a spectrally smooth broadband laser for the probe laser and performing multiplex NDFWM by dispersing the signal beam with a high-resolution interferometer. A similar technique has been demonstrated and analyzed for DFWM, where spectra of OH were obtained with a single laser pulse [11].

4 Conclusion

We have demonstrated a new technique for gas-phase velocimetry based on NDFWM. Our experimental results compare well with theoretically calculated velocities and are consistent with measurements based on laser-induced fluorescence. While LIF velocimetry is simpler and capable of providing instantaneous velocity flow-fields, NDFWM may be attractive for applications involving limited optical access, luminous or harsh environments, or non-fluorescing molecules.

Acknowledgements. We gratefully acknowledge the contributions of Brandon Yip at the Physikalisch-Chemisches Institut, Universität Heidelberg, Germany; and David Chandler, Eric Rohlfing and Forest Blair at the Combustion Research Facility, Sandia National Laboratories, Livermore, CA. This work was supported by the U.S. Department of Energy, Office of Basic Energy Sciences, Division of Chemical Sciences. Funding for PMD was provided by the Air Force Office of Scientific Research, Aerospace Sciences Directorate.

References

1. E.O. Doebelin: *Measurement Systems: Application and Design*, 4th edn. (McGraw-Hill, New York 1990)
2. L.M. Lourenco, A. Krothapalli, C.A. Smith: In *Advances in Fluid Mechancis Measurements*, ed. by M. Gad-El-Hak (Springer, Berlin, Heidelberg 1989) p. 606
3. R.B. Miles, D. Zhou, B. Zhang, W. Lempert, Z.S. She: A.I.A.A. J. **31**, 447–452 (1993)
4. See for example, D.F. Davidson, A.Y. Chang, M. D. Di Rosa, R.K. Hanson: Appl. Opt. **30**, 2598–2608 (1991) and references therein
5. M.D. Di Rosa, A.Y. Chang, R.K. Hanson: Appl. Opt. **32**, 4074–4087 (1993)
6. J.L. Palmer, B.K. McMillin, R.K. Hanson: A.I.A.A. Paper 92-0762 (1992)
7. R.B. Miles, W. Lempert: Appl. Phys. B **51**, 1–7 (1990)
8. M. Lefebvre, M. Pealat, J. Strempel: Opt. Lett. **17**, 1806–1808 (1992)
9. R.B. Williams, P. Ewart, A. Dreizler: Opt. Lett. **19**, 1486–1488 (1994)
10. C.H. Kruger, C.O. Laux, R.J. Gessman: A.I.A.A. J. (submitted)
11. D.R. Meacher, A. Charlton, P. Ewart, J. Cooper, G. Alber: Phys. Rev. A **42**, 3018–3026 (1990)
12. J. Nilsen, A. Yariv: J. Opt. Soc. Am. **71**, 180–183 (1981)
13. W. Demtröder: *Laser Spectroscopy*, 2nd edn. (Springer, Berlin, Heidelberg 1995)
14. D.R. Miller: In *Atomic and Molecular Beam Methods*, ed. by G. Scoles (Oxford Univ. Press, Oxford 1988) pp. 14–53
15. R.L. Farrow, D.J. Rakestraw: Science **257**, 1894–1900 (1992)